Some advances on inverse particle transport problems with applications to homeland security

Gregory Thoreson[1], Jean C. Ragusa[1], Wolfgang Bangerth[2]

Texas A&M University, [1]Dept. of Nuclear Engineering, [2]Dept. of Mathematics
College Station, TX 77843-3133, USA
E-mails: gthoreson@tamu.edu ; ragusa@ne.tamu.edu, bangerth@math.tamu.edu

INTRODUCTION

Generally speaking, inverse problems consist of the recovery of coefficients in a domain from data in the domain (invasive inverse problems) and/or data on its boundaries (noninvasive inverse problems). In particle inverse problems, photons (including X-rays), neutrons or both are used. The most commonly found inverse problems include computed tomography/radiography with applications to medical fields, oceanography, homogenization, aerospace engineering, object detection (including special nuclear material, chemical or biological agents) etc [1,2,3]. For instance, tomographic imaging is a non-contact, non-destructive investigation method that provides cross-sectional images of objects from transmission data measured by illuminating the objects from one or more different directions and locations. A set of mathematical techniques reconstruct (i.e., infer) the composition of the interior of the objects from their cross-sectional images. The common feature of these so-called inverse problems is that the unknowns are the object material properties and the givens are the data collected when illuminating the object with a known source. Data can be collected inside the object (invasive method) or at its boundaries (noninvasive method). For the purpose of homeland security applications, such as cargo and container screening, we will mostly consider noninvasive inverse problems where measurements are performed at the boundaries of the object under scrutiny. The uniqueness of solutions for such problems is discussed in [5,6]; noninvasive problems have in general no unique solution except in the case of 1-group transport with isotropic of mildly anisotropic scattering (see [6]).

An unconstrained optimization approach combined with duality principles was previously devised to solve the noninvasive inverse problem [7]. In this paper, we show equivalence of solutions of the previous unconstrained optimization framework with a more conventional constrained optimization approach. We also provide 1-group 2-D sensitivity studies for a sarin vile hidden in a high scatterer object.

THEORY

The noninvasive reconstruction problem is a nonlinear optimization problem. It consists of finding the distribution of the optical properties Σ of the object under investigation so that the neutron fluxes recovered at the boundary ∂X of the domain X best match the measured fluxes. We briefly recall earlier results based on the unconstrained problem, describe the constrained problem, and show the equivalence between these two frameworks.

Unconstrained minimization problem

Assuming that some initial guess of the material property is given, one computes the functional F measuring the discrepancy between the predicted particle fluxes $\Psi(\Sigma)$ at the boundary, obtained by solving the transport equation, and the measured fluxes Ψ^* . The functional F to be minimized reads as follows:

$$F\left(\Sigma,\Psi(\Sigma)\right)=\frac{1}{2}\int_0^\infty dE\int_{\partial X} dS\int_{\vec{\Omega}\cdot\vec{n}>0} d\Omega\boldsymbol{\Omega}\cdot\mathbf{n}\left[\Psi(\Sigma)-\Psi^*\right]^2 \quad (1).$$

Tikhonov regularization terms could be added to F to ensure existence of a solution; we omit them here solely for clarity in demonstrating the equivalence between the two frameworks. Furthermore, for conciseness, we define $\left\langle f,g\right\rangle_\pm=\int_{\Gamma\pm} d_b x\, fg$ where $d_b x = dSdEd\Omega\left|\boldsymbol{\Omega}\cdot\mathbf{n}\right|$ and $\Gamma\pm=\partial X\times\left[0,\infty\right]\times\left(2\pi\right)_\pm$, hence we have:

$$F\left(\Sigma,\Psi(\Sigma)\right)=\frac{1}{2}\left\langle\Psi(\Sigma)-\Psi^*,\Psi(\Sigma)-\Psi^*\right\rangle_+ \quad (2).$$

Once the functional has been defined and an initial guess for the material properties has been chosen, a direct problem

$$\left\{B\Psi=S \text{ on } D,\ \Psi=\Psi^{inc} \text{ on } \Gamma-\right\} \quad (3)$$

is solved for flux $\Psi(\Sigma)$ due to an extraneous source S, if any, and an incident flux Ψ^{inc} (the illuminating source). $B=\boldsymbol{\Omega}\cdot\nabla+\Sigma-H-P$ is the transport operator, with H the scattering operator and P the production operator. The phase-space is $D=X\times\left[0,\infty\right]\times\left(4\pi\right)$. If the value of the misfit function for this $\Psi(\Sigma)$ is zero, then the material properties are the correct converged values. Otherwise, we need to update the material properties using an iterative method. This is done by evaluating the gradient of this functional with respect to the material properties, i.e., $\nabla_\Sigma F$, which indicates how material properties influence the particle fluxes. This gradient is:

$$\nabla_\Sigma F=\left\langle\partial_\Sigma\Psi(\Sigma),\Psi(\Sigma)-\Psi^*\right\rangle_+ \quad (4).$$

Using duality principles [4,3], Eq. 4 is replaced by:

$$\nabla_\Sigma F=\left(\Psi^\dagger(\Sigma),(\partial_\Sigma B)\Psi(\Sigma)\right) \quad (5)$$

where $\left(f,g\right)=\int_D dx\, fg$ with $dx = dSdEd\Omega$ and $\Psi^{\dagger}(\Sigma)$ is the adjoint flux, solution of the adjoint problem

$$\left\{B^{\dagger}\Psi^{\dagger}=0 \text{ on } D,\ \Psi^{\dagger}=\Psi(\Sigma)-\Psi^{*} \text{ on } \Gamma+\right\} \qquad (6).$$

Because the leakage term in B is absent from $\partial_{\Sigma}B$, Eq. 5 is a simple integral to compute.

Constrained minimization problem

An alternative viewpoint is to write the problem as a constrained minimization problem, where the objective functional is written as:

$$\tilde{F}\left(\Sigma,\Psi\right)=\frac{1}{2}\left\langle \Psi-\Psi^{*},\Psi-\Psi^{*}\right\rangle_{+} \qquad (7)$$

and where the explicit dependence of Ψ on Σ has been removed. Rather, this dependence is expressed as a constraint in the form of Eq. 3. To solve the constrained problem, we introduce the Lagrangian functional L

$$\begin{aligned} L(\Sigma,\Psi,\lambda) = &\frac{1}{2}\left\langle \Psi-\Psi^{*},\Psi-\Psi^{*}\right\rangle_{+} \\ &+\left(\lambda, B\Psi-S\right)+\left\langle \lambda,\Psi-\Psi^{inc}\right\rangle_{-} \end{aligned} \qquad (8)$$

where λ is the Lagrange multiplier acting on the constraint (the direct transport problem). From the theory of constrained optimization, we know that the optimum satisfies the following optimality condition for L

$$\frac{\partial L}{\partial \Sigma}=0;\ \ \frac{\partial L}{\partial \Psi}=0;\ \ \frac{\partial L}{\partial \lambda}=0; \qquad (9).$$

At any iteration during the optimization process, it is easy to note

1. that the first equality in Eq. 9 leads to Eq. 5 (previously obtained from Eq. 4 via duality principles),
$$\frac{\partial L}{\partial \Sigma}=\left(\lambda,(\partial_{\Sigma}B)\Psi\right) \qquad (10)$$
2. that the second equality in Eq. 9 leads naturally to Eq. 6 (and that the Lagrange multiplier is simply the adjoint flux),
$$\frac{\partial L}{\partial \Psi}=\left(1,B^{\dagger}\lambda\right)+\left\langle 1,\lambda+\Psi-\Psi^{*}\right\rangle_{+} \qquad (11)$$
3. and that the third equality in Eq. 9 is simply related to Eq. 3 (the constraint itself).
$$\frac{\partial L}{\partial \lambda}=\left(1,B\Psi-S\right)+\left\langle 1,\Psi-\Psi^{inc}\right\rangle_{-} \qquad (12).$$

Should the functional $\tilde{F}$ be equal to zero, the optimality condition Eq. 9 would necessarily be satisfied because the misfit $\Psi-\Psi^{*}$ would be exactly 0, leading to a null Lagrange multiplier in Eq. (11), and thus a null RHS in Eq. (10).

Consequently, solutions to the unconstrained problem are also solutions to the constrained one, and vice versa.

On the other hand, while in the unconstrained case the coefficient Σ is the only variable that is updated in each iteration (while the flux and adjoint flux are then recomputed using Eqs. 3 and 6), in the constrained case all three of these variables are considered independent and are updated independently using the gradient of L defined in Eq. 9. While the result of this is that the flux and adjoint flux do not satisfy the forward and adjoint equation at each iteration (though they do at the point of the solution), decoupling the functional F and the state equation typically leads to a less nonlinear and consequently simpler to solve problem.

SENSITIVITY STUDIES

Before implementing the proposed methodologies for the noninvasive inverse problem, it is worthwhile testing whether material property changes within the domain would cause a reasonable signal at the boundaries. A model of a 2-D 100 cm^2 square container (wood, aluminum, polyethylene) containing various inclusions (Cobalt or sarin nerve gas) was used. An incoming neutron flux was applied on one side and measurements were taken on all four sides. The inclusions were moved within the container. A S_{16} 1-group bilinear short characteristics method was used to solve the transport equation. The sensitivities and relative sensitivities are calculated as

$$\frac{\left\|\Psi(\Sigma_A)-\Psi(\Sigma_B)\right\|}{\left\|\Sigma_A-\Sigma_B\right\|} \text{ and } \frac{\left\|\Psi(\Sigma_A)-\Psi(\Sigma_B)\right\|}{\left\|\Sigma_A-\Sigma_B\right\|}\frac{\left\|\Sigma_A\right\|}{\left\|\Psi(\Sigma_A)\right\|} \qquad (13)$$

by solving several forward problems. The case of 1 cm^2 sarin gas vile is presented in figures 1 and 2. The x and y coordinates represent the inclusion location. Regardless of the inclusion position, significant sensitivity values can be noted on at least one side of the object. By illuminating the object from more than just one side, sensitivities are expected to be even greater.

CONCLUSION and ONGOING WORK

Computed tomography based on the full transport equation can be readily applied in a mathematically consistent fashion, either as an unconstrained optimization problem devised with the help of duality relations or as a constrained optimization problem. Both frameworks yield equivalent solutions, though their implementation complexity, convergence properties, and effectiveness may differ; for instance, the constrained formulation solves both the forward transport problem and the minimization problem at once. These methodologies are presently developed for national security applications (neutron radiography of devices, detection of special nuclear material in cargos and containers, etc.).

REFERENCES

1. S.R. Arridge ,"Optical tomography in medical imaging", *Inverse Problems* **15** No 2 (1999)

2. N.J. McCormick,“"Inverse radiative transfer problems: a review," *Nucl. Sci. Eng.* ***112***, 185-198 (1992).”
3. J. Ragusa, R. Sanchez, S. Santandrea, “A Technique for Reflector Homogenization”, *Mathematics and Computation, Supercomputing, Reactor Physics and Nuclear and Biological Applications*, Palais des Papes, Avignon, France, September 12-15, 2005
4. R. Sanchez, “Duality, Green’s functions and all that”, *Transport Theory and Statistical Physics*, **27**, 445 (1998)
5. R. Sanchez and N. J. McCormick, “Inverse Source Problems in Linear Transport Theory”, *Trans. Am. Nucl. Soc*., ANS Meeting, Albuquerque, NM, USA, November 2006.
6. R. Sanchez and N. J. McCormick, *Inverse Problems* (submitted, 2006). Personal communication of R. Sanchez.
7. J. Ragusa, “Application of duality principles to solve inverse particle transport problem: a framework”, *Trans. Am. Nucl. Soc*., ANS Meeting, Washington DC, USA, November 2005.

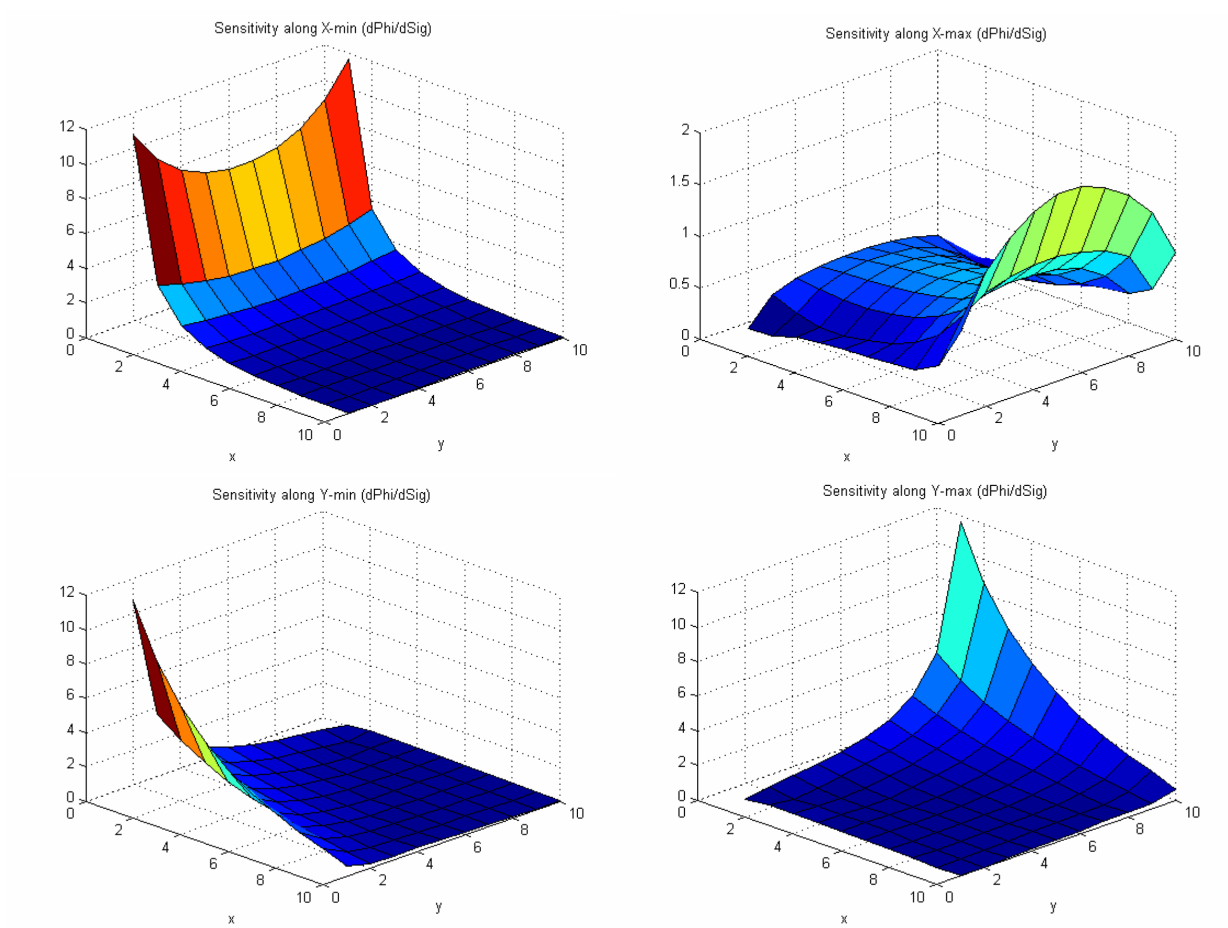

Fig. 1. Sensitivities as a function as the position of a sarin gas vile in wooden container. The plots show the relative change in neutron flux after illumination from the left for different positions of the inclusion when measuring the flux on the left (top left image), right (top right), front (bottom left), and back (bottom right) boundaries, respectively.

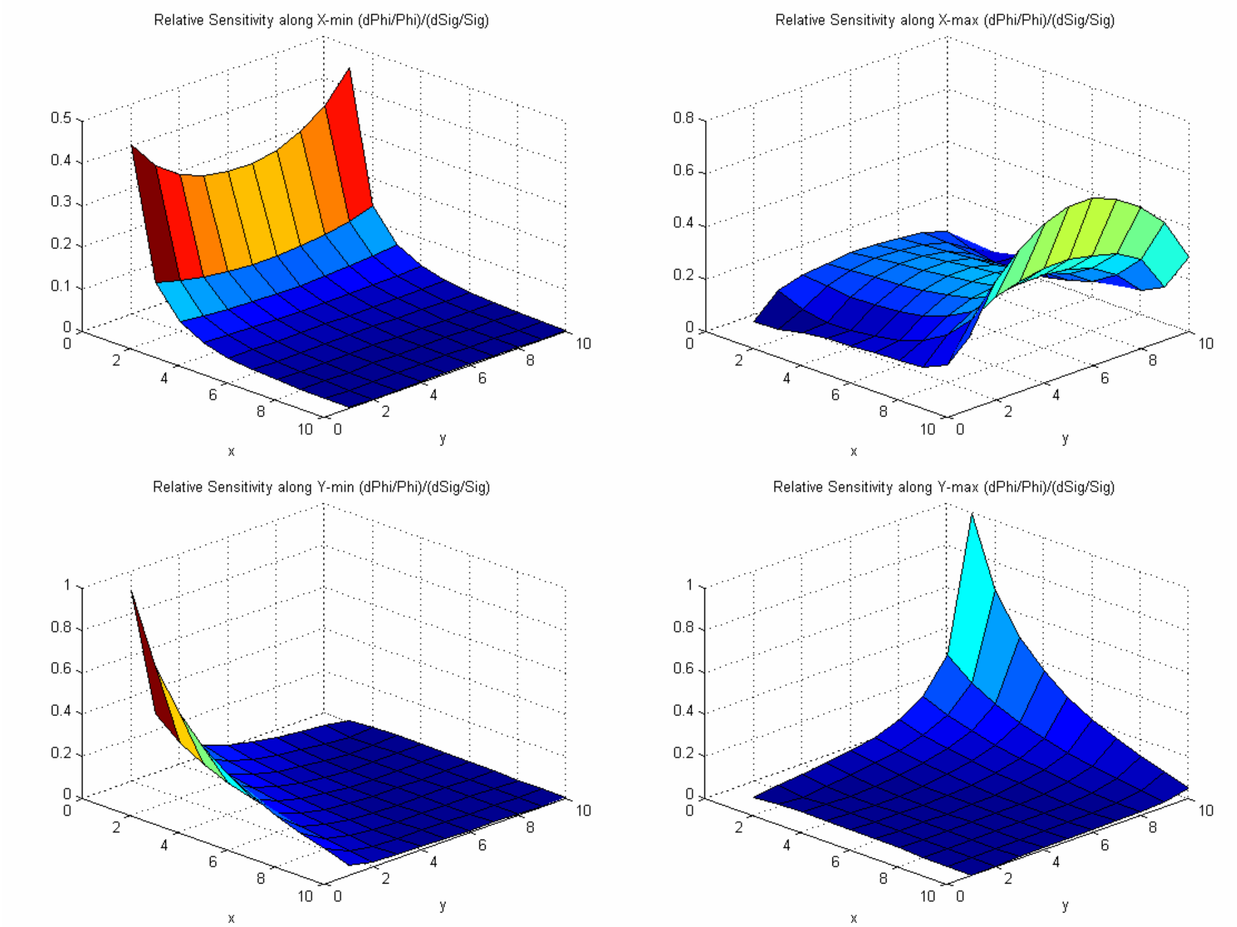

Fig. 2. Relative sensitivities as a function as the position of a sarin gas vile in wooden container. The plots show the relative change in neutron flux after illumination from the left for different positions of the inclusion when measuring the flux on the left (top left image), right (top right), front (bottom left), and back (bottom right) boundaries, respectively.